Phase diagram of three contrasting magnetization reversal phases in uniaxial ferromagnetic thin films

Sug-Bong Choe[a] and Sung-Chul Shin
Department of Physics and Center for Nanospinics of Spintronic Materials, Korea Advanced Institute of Science and Technology, Taejon 305-701, Korea

(Received 12 June 2001; accepted for publication 4 January 2002)

We present an analytical description of a magnetization reversal phase diagram of ferromagnetic thin films that have uniaxial perpendicular anisotropy. The phase equilibrium lines were calculated from a micromagnetic consideration of equilibrium conditions of the wall motion, dendritic growth, and nucleation processes. The phase diagram characterizes well simulated domain evolution patterns: typical domain evolution patterns are predicted accurately in the corresponding phases accompanied by gradual phase transitions across the phase equilibrium lines. © *2002 American Institute of Physics.* [DOI: 10.1063/1.1457527]

Motivated by the diverse possibilities of magnetic applications as well as a fundamental interest in magnetism, magnetization reversal dynamics in ferromagnetic thin films have been extensively studied during the last few decades.[1–3] Recently, interest in this field has grown significantly, largely motivated by experimental observations of contrasting domain patterns among similar samples of many systems.[4–7] Direct domain observation using advanced magnetic imaging techniques has shown that the contrasting domain patterns resulted from the counterbalance of three fundamental magnetization reversal processes: nucleation, dendrite-growth, and wall-motion processes.[4,7] Micromagnetic calculations have indeed demonstrated the contrasting change of simulated domain evolution patterns with respect to the magnetic properties.[7–13]

Kirby *et al.*[8] first presented simulated results of contrasting behavior from wall motion to nucleation-dominant magnetization reversal with respective to the domain wall energy, which could explain the experimental observations in Dy/Fe multilayers well. Lyberatos *et al.*[9] developed a more generalized micromagnetic description of magnetization reversal, which predicted three contrasting behaviors among the wall-motion, nucleation, and dendritic-growth processes depending on the magnetic properties of samples. Several equivalent models have been reported to explain the magnetization reversal behavior observed in a number of different sample systems,[7,10] taking into consideration the local magnetic variation.[11,12] Quite recently, Lyberatos[13] summarized the various micromagnetic algorithms and their relevancy for each physical situation.

Despite these advances, however, we would like to point out that in all of the existing micromagnetic approaches, the simulated results can only be obtained after time-consuming iterative calculations. This essentially restricts the scope of potential research to some particular cases, especially those on areas much smaller than experimental-observed areas because the simulation time rapidly increases with an increase in the simulation area, i.e., the number of simulation cells. Thus, an explicit characterization of magnetization reversal behavior without carrying out a time-consuming iterative simulation remains a scientific challenge to date.

In this study, we present an analytic description of magnetization reversal behavior based on a micromagnetic model of uniaxial perpendicular magnetic anisotropy. The description provides a magnetization reversal phase diagram determined from equilibrium conditions of typical magnetization reversal processes. The validity of this phase diagram is discussed together with simulated domain evolution patterns.

For this study, a micromagnetic model was developed to predict the magnetization reversal dynamics by adopting a Monte Carlo algorithm based on a uniaxial anisotropy model originally proposed by Kirby *et al.*[8] In this model, a film is composed of nanosized identical single-domain cells on hexagonal lattices lying in an *XY* plane with periodic boundary condition, and the magnetization of each cell is aligned along the $\pm z$ direction except during the reversal process. Each cell of volume V_c has a saturation magnetization of M_s and a uniaxial perpendicular magnetic anisotropy of K_u, and each cell boundary has a wall energy density σ_w. Then, the magnetic energy E of a cell having an angle of magnetization direction θ from the $+z$ axis is given by

$$E = \left.\begin{aligned} K_u V_c \sin^2\theta - M_s V_c (H+\hat{H})\cos\theta \\ +2(1-\zeta\cos\theta) V_c \sigma_w / d_c \end{aligned}\right\}, \tag{1}$$

where H and $\hat{H}$ are the external magnetic field and the demagnetizing field along the $+z$ direction, respectively. $\zeta = \Sigma_k \cos\theta_k/6$ is the fraction of the magnetization state summed over the nearest neighboring cells k, and d_c is the distance between the centers of the nearest neighboring cells. The magnetic energy can be rewritten into a simplified form expressed by

$$E = K_u V_c [\sin^2\theta - 2(\alpha + m\hat{h} + \zeta w)\cos\theta + 2w], \tag{2}$$

introducing the dimensionless parameters where $m = 2\pi M_s^2/K_u$ is the ratio of the magnetostatic energy over the anisotropy energy, $w = \sigma_w/t_c K_u$ is the ratio of the wall energy over the anisotropy energy, $\alpha = M_s H/2K_u$ is the ratio of

[a]Presently at: Advanced Light Sources, Lawrence Berkeley National Laboratory; electronic mail: SBChoe@lbl.gov

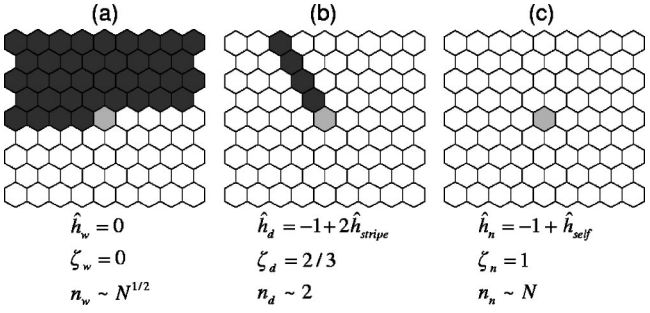

FIG. 1. Typical situations of (a) the wall-motion process, (b) the dendritic-growth process, and (c) the nucleation process, respectively. The magnetization reversal situation parameters, $\hat{h}$, ζ, and n, for the corresponding magnetization reversal situations are given at the bottom for each case. Here, $\hat{h}_{\text{stripe}}$ is the contribution to the demagnetizing energy from the cells lying on the linear stripe domain, shown as black cells in (b), and $\hat{h}_{\text{self}}$ is the self-demagnetizing energy of a cell.

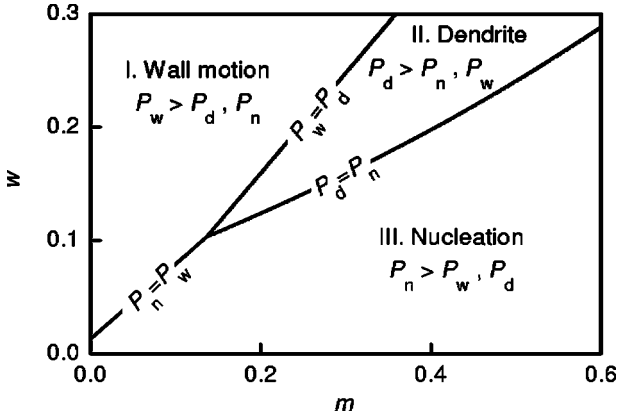

FIG. 2. Phase diagram of the wall-motion dominant phase (partition I), the dendritic-growth dominant phase (partition II), and the nucleation dominant phase (partition III). The solid lines provide the phase equilibrium lines under the condition denoted on the corresponding lines.

the applied magnetic field over the anisotropy field and $\hat{h} = \hat{H}/4\pi M_s$ is the ratio of the demagnetizing field over its maximum value.

The magnetic energy E has two minima at $\theta = 0$ and π with a maximum in between. The energy barrier E_b for reversal is then given by the difference in energy between the initial value and the maximum as follows:

$$E_b = K_u V_c [1 + \hat{m}(\alpha + m\hat{h} + \zeta w)]^2, \tag{3}$$

where $\hat{m} = \cos\theta_0$ is the directional cosine of the initial magnetization direction θ_0 of the cell. In a thermally activated magnetization reversal process, magnetization reversal of a cell takes place by overcoming the energy barrier E_b via activation with the thermal energy $k_B T$, and the switching probability of a cell in time Δt is given by

$$p = r_0 \exp(-\beta'[1 + \hat{m}(\alpha + m\hat{h} + \zeta w)]^2)\Delta t, \tag{4}$$

where r_0 is the probability constant (or inverse of the attempt frequency). Here, $\beta' = K_u V_c / k_B T$ is another dimensionless parameter that gives the ratio of the magnetic anisotropy energy of a cell over the thermal activation energy.

The switching probability p of an individual cell is determined according to the magnetization state of the neighboring cells. Now we consider typical situations of the three fundamental magnetization reversal processes illustrated in Fig. 1: the wall-motion process takes place by switching a cell at the boundary of an existing domain; the dendritic-growth process switches a cell at the end of a stripe domain; the nucleation process makes an isolated cell. From the typical situations, one can determine the situation parameters, i.e., the normalized demagnetizing field $\hat{h}$ and the domain-wall coverage ζ according to the corresponding magnetization reversal process. The values of the situation parameters are given at the bottom of each part in Fig. 1. The number of cells n in each typical situation was chosen as an approximate quantity.

The probability P_i, where the magnetization reversal process i takes place among all of the simulation cells, is given by the sum of the individual switching probability p_i of the number of cells n_i in a typical situation of the magnetization reversal process i, i.e., $P_i \sim n_i p_i$. The equilibrium condition between the magnetization reversal processes i and j is then given by $P_i = P_j$, since the subsequent magnetization reversal is chosen by a counterbalance between the probabilities of the magnetization reversal processes. Using Eq. (4), the equilibrium condition can be rewritten as a function between the normalized domain-wall energy w and the normalized magnetostatic energy m, given by

$$w(m) = \frac{-b_{ij} + \sqrt{b_{ij}^2 - a_{ij}c_{ij}}}{a_{ij}}, \tag{5}$$

where the coefficients a, b, and c are

$$a_{ij} = \zeta_i^2 - \zeta_j^2,$$

$$b_{ij} = (\hat{h}_i\zeta_i - \hat{h}_j\zeta_j)m + (1+\alpha)(\zeta_i - \zeta_j),$$

$$c_{ij} = (\hat{h}_i^2 - \hat{h}_j^2)m^2 + 2(1+\alpha)(\hat{h}_i - \hat{h}_j)m - \frac{1}{\beta'}\log\frac{n_i}{n_j}.$$

In this study, w and m are chosen as major quantities due to the fact that they directly reflect the different magnetization reversal situations to the reversal probability via the term $m\hat{h} + \zeta w$ in Eq. (4), whereas the other parameters, such as α, β', and N, just give the same contribution to all the reversal probability; more detailed discussion of this will be reported elsewhere.

Figure 2 shows the phase equilibrium lines on the $m-w$ coordinate, where each line is designated by a corresponding equilibrium condition. Here, the other parameters are fixed to $\beta' = 837$ and $\alpha = -0.75$ on 256×256 cells. The value of β' corresponds to the values of $K_u = 5 \times 10^6$ erg/cm^3, $t_c = t_f = 2 \times 10^{-6}$ cm, and $T = 300$ K. From Fig. 2, one can clearly see the phase diagram is composed of three magnetization reversal phases. In phase I, the wall-motion process is dominant compared to the other processes, i.e., $P_w > P_d$ and P_n, whereas the dendritic-growth process is dominant in phase II and the nucleation process is dominant in phase III.

To examine whether the phase equilibrium lines accurately classify the magnetization reversal phases, a micromagnetic simulation was carried out under conditions identical to those used in the present phase diagram. Figure 3 illustrates the simulated domain evolution patterns with respect to m and w together, where each frame is aligned in a column with different m and in a row with different w. Each frame shows a domain evolution pattern of 25% reversal for

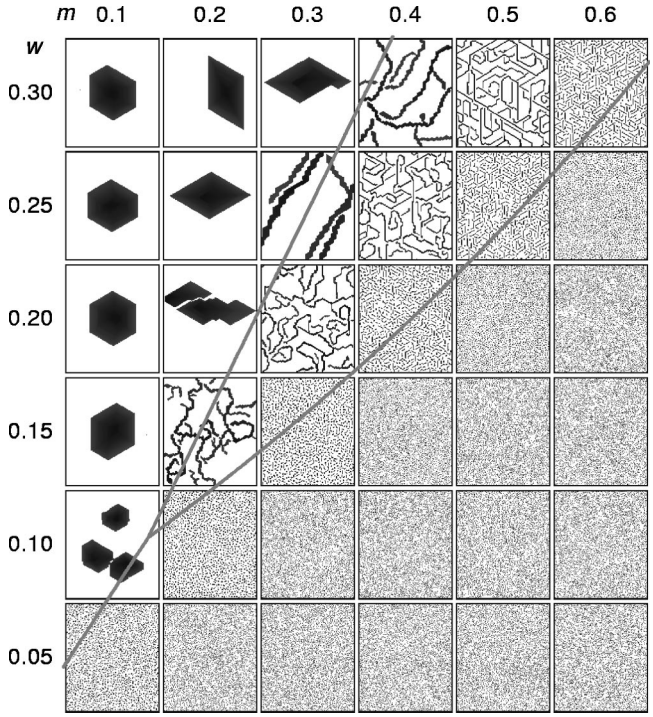

FIG. 3. Simulated domain evolution patterns with respect to the magnetostatic energy m and the domain-wall energy w. Each frame is aligned in a column with m and in a row with w, which shows a domain evolution pattern of 25% reversal for a sample having the corresponding value of m and w denoted in the top and left margins of the array, respectively. The gray lines show the phase equilibrium lines determined by Eq. (5).

a sample having corresponding values of m and w as denoted in the top and left margins of the domain-pattern arrays, respectively. All the domain evolution patterns systematically change with a change in either m or w, and one can clearly find three peculiar domain patterns: (i) a large domain; (ii) dendrite-like stripe domains; (iii) small nucleated domains. It should be pointed out that the fundamental characteristics of these domain evolution patterns are basically unchanged with respect to the time elapsed (or the reversal percentage), and thus they can be considered as invariant features closely related to the quasiground energy state of the static domain patterns.

We plot the phase equilibrium lines together with the simulated domain evolution patterns shown by the gray lines in Fig. 3. It is clear that the domain evolution patterns are classified well by the phase diagram: all the domain evolution patterns of each extreme phase appear inside the corresponding partition, whereas the intermediate patterns are seen around the phase equilibrium lines.

An intriguing question we would like to address concerning the phase transition behavior across the phase equilibrium lines is whether the magnetization reversal process exhibits an abrupt transition or a smooth transition with different magnetic properties. A detailed investigation of the domain evolution patterns around the phase equilibrium lines revealed that all the phase transitions were preceded by continuous changes in domain evolution patterns. For instance, a phase transition with a change in w across the phase equilibrium line exhibits a gradual change in magnetization reversal dynamics between the wall-motion dominant phase and the nucleation dominant phase: the average size of the domains gradually increases while the number of domains gradually decreases with an increase in w. A smooth phase transition was also observed between the wall-motion dominant phase and the dendritic-growth dominant phase with a change in m across the phase equilibrium line.

Note that the present phase diagram was calculated from only three extreme situations of typical magnetization reversal processes. But there are other intermediate situations, such as wall motion from a curved domain boundary, dendritic growth from a thick stripe, or nucleation near existing domains. The situation parameters of these intermediate processes have their own values, and therefore additional minor phase equilibrium lines between these intermediate processes possibly exist. Thus, it is expected that the magnetization reversal dynamics gradually change with changes in the magnetic properties via successive minor phase transitions across every intermediate phase equilibrium line, for instance, from thinner stripe domains to thicker stripe domains, and finally to a large circular domain.

In summary, we presented an analytical prediction of the magnetization reversal phase diagram by micromagnetic consideration of uniaxial ferromagnetic thin films. The phase equilibrium lines were calculated by considering the extreme cases of three contrasting magnetization reversal processes: wall-motion, dendritic growth, and nucleation processes. The phase diagram was able to characterize the simulated domain evolution patterns accompanied by gradual phase transitions across the phase equilibrium lines well and, thus, it provides a good explicit prediction of magnetization reversal phase without having to carry out any time-consuming iterative simulation.

This work was supported by the Korean Ministry of Science and Technology through the Creative Research Initiative Project.

[1] J. L. Simonds, Phys. Today **48**, 26 (1995).
[2] K. M. Krishnan, MRS Bull. **20**, 24 (1995).
[3] G. A. Prinz, Science **282**, 1660 (1998).
[4] J. Pommier, P. Meyer, G. Pónissard, J. Ferré, P. Bruno, and D. Renard, Phys. Rev. Lett. **65**, 2054 (1990).
[5] A. Kirilyuk, J. Ferré, J. Pommier, and D. Renard, J. Magn. Magn. Mater. **121**, 536 (1993).
[6] J. Ferré, V. Grolier, P. Meyer, S. Lemerle, A. Maziewski, E. Stefanowicz, S. V. Tarasenko, V. V. Tarasenko, M. Kisielewski, and D. Renard, Phys. Rev. B **55**, 15092 (1997).
[7] S.-B. Choe and S.-C. Shin, Phys. Rev. B **57**, 1085 (1998); **62**, 8646 (2000).
[8] R. D. Kirby, J. X. Shen, R. J. Hardy, and D. J. Sellmyer, Phys. Rev. B **49**, 10810 (1994).
[9] A. Lyberatos, J. Earl, and R. W. Chantrell, Phys. Rev. B **53**, 5493 (1996).
[10] U. Nowak, J. Heimel, T. Kleinfeld, and D. Weller, Phys. Rev. B **56**, 8143 (1997).
[11] A. Lyberatos, J. Magn. Magn. Mater. **186**, 248 (1998).
[12] S.-B. Choe and S.-C. Shin, IEEE Trans. Magn. **36**, 3167 (2000).
[13] A. Lyberatos, J. Phys. D **33**, R117 (2000).